PHYSICAL REVIEW B VOLUME 52, NUMBER 20 15 NOVEMBER 1995-II

# Thermal carrier emission from a semiconductor quantum well

S. Weber, W. Limmer, K. Thonke, and R. Sauer
*Abteilung Halbleiterphysik, Universität Ulm, 89069 Ulm, Germany*

K. Panzlaff*
*Abteilung Optoelektronik, Universität Ulm, 89069 Ulm, Germany*

G. Bacher
*Technische Physik, Universität Würzburg, Am Hubland, 97074 Würzburg, Germany*

H. P. Meier and P. Roentgen
*IBM Forschungszentrum Zürich, Säumerstrasse 4, CH 8803 Rüschlikon, Switzerland*
(Received 7 April 1995; revised manuscript received 11 July 1995)

The intensity and the lifetime of quantum well (QW) photoluminescence (PL) both decrease at high temperatures. This is ascribed to thermal emission of charge carriers out of confined QW states into barrier states and subsequent nonradiative recombination processes. Corresponding activation energies reported in several publications range from the total QW binding energy $\Delta E_{\text{tot}}$ of electrons and holes to half of $\Delta E_{\text{tot}}$, or to the binding energy of the shallower bound particle. In pursuit of this discrepancy, we perform steady-state and time-resolved PL measurements under high- and low-excitation conditions on a series of multiple QW structures of the material systems $In_xGa_{1-x}As/GaAs$, $GaAs/Al_xGa_{1-x}As$ , and $In_xGa_{1-x}As/InP$. Covering an intensity range of more than three orders of magnitude, we find that in the high-temperature limit the final activation is associated with $\Delta E_{\text{tot}}$ for both high and low excitation. We discuss our findings in the frame of a simple model for the density of states, thermalization, and recombination rates of electrons and holes.

## I. INTRODUCTION

During recent years great interest has been focused on the dynamics of photoexcited carriers in single quantum well and multiple quantum well (MQW) structures. The electron-hole pairs created in the barrier region rapidly thermalize through interaction with phonons and are trapped into confined QW states. From there they recombine radiatively and nonradiatively. The intensity and effective lifetime of QW photoluminescence (PL) are strongly temperature dependent and decrease with increasing temperature. Two main PL loss mechanisms have been alternatively discussed: The first mechanism is the thermally activated recombination by traps, presumably located at the interface between barrier and QW.[1–6] The second one is the thermal escape of charge carriers from confined QW states into barrier states followed by effective nonradiative recombination there.[7–20] Recent observations suggest that the second process is dominating: With increasing temperature PL from the barrier[12,14] and a vertical transport of charge carriers between adjacent QW's (Refs. 11, 15, 17, and 18) has been detected that is governed by the same activation energy as the decrease of the QW PL intensity. Furthermore, the loss of QW PL intensity can be strongly reduced by growing additional cladding barriers[17] preventing the charge carriers from leaving the QW region. Despite the large number of studies dealing with carrier recombination in QW structures, no general agreement has yet been achieved on the characteristic energy for the carrier emission. Gurioli and co-workers[7,8] find with time-resolved (TR) PL measurements an activation energy for the nonradiative recombination process equal to the binding energy of electrons or holes, whichever is smaller. They claim that only TR measurements are able to obtain correct activation energies. Michler *et al.*[9] and Bergman *et al.*[10] from their TR PL investigations derive an activation energy equal to half of the total binding energy $\Delta E_{\text{tot}}$ in the QW. Other groups from both continuous-wave (CW) and TR PL experiments[11,13–17] conclude that the thermal PL quenching is governed by the total binding energy $\Delta E_{\text{tot}}$. Michler *et al.*[9] suggested that this controversy could be due to different excitation densities (high injection vs low injection) involved in the experiments.

In this paper we report a photoluminescence study under CW and picosecond excitation of strained and lattice-matched $In_xGa_{1-x}As/GaAs$ with $x$=10% and 15%, $In_{0.53}Ga_{0.47}As/InP$, and $Al_{0.33}Ga_{0.67}As/GaAs$ MQW structures. Covering a PL intensity range of more than three orders of magnitude, we show that in the high-temperature limit the main activation energy obtained by both CW and TR PL measurements is associated with the sum of the binding energies of electrons and holes. This is in contrast to the statement of Gurioli *et al.*[7,8] Since the four samples under investigation belong to different material systems and QW structures, this result is supposed to be of general validity. Our experimental findings are confirmed by theoretical considerations. Here, a concept is chosen that includes confined two-dimensional (2D) states in the QW and unbound three-dimensional (3D)-like states above the QW. The recombination rates

 ©1995 The American Physical Society

are set proportional to the electron and hole densities as required for bimolecular recombination. This leads to a quadratic and a linear term in the excess carrier densities that are both important when low and high excitation conditions are modeled. In this respect our procedure is different from that of Michler *et al.*,[9] who assume a recombination term only linear in the excess carrier density. Further, it is essential in the present considerations that the confined electron and hole densities in a QW need not be equal since their individual binding energies can be different and quasithermal equilibrium between confined and unbound QW states is assumed. The case of $n$-type material is discussed in detail, and it is demonstrated that no qualitative difference in the temperature dependence of PL intensity or lifetime is expected between high and low excitation densities.

## II. THEORETICAL CONSIDERATIONS

In this section we develop a simple theoretical model, describing the temperature and time dependence of the QW photoluminescence intensity $I_{\rm PL}$. It is based on the assumption that charge carriers are distributed in energy according to Fermi-Dirac statistics. Considering a single rectangular QW with confinement energies $E_i$ $(i = 1, \dots, l-1)$ and well potential depth $E_l$ we define sheet charge carrier densities $N_i$ and $N_l$ by

$$N_i = \int_{E_i}^{E_{i+1}} D^{\rm 2D}(E) f(E,T) dE \ , \quad i < l, \tag{1}$$

$$N_l = \int_{E_l}^{\infty} D^{\rm 2D}(E) f(E,T) dE \ , \tag{2}$$

where $D^{\rm 2D}(E)$ denotes the corresponding 2D density of states (DOS) and $f(E,T)$ the quasiequilibrium Fermi-Dirac distribution due to the optical excitation. According to these definitions $N_i$ $(i < l)$ represents the temperature-dependent density of confined charge carriers with energies in the range $E_i \le E \le E_{i+1}$. $N_l$ denotes the concentration of charge carriers that occupy unbound states with energies above the potential barrier $E_l$. For energies below $E_l$ the DOS is supposed to have the usual steplike form for 2D bands. Above $E_l$, with the contribution of 3D states, a square-root energy dependence is assumed:

$$D^{\rm 2D}(E) = \sum_{i=1}^{l-1} \frac{c_i}{k_B} \theta(E - E_i) + \frac{c_l}{k_B^{3/2}} (E - E_l)^{1/2} \theta(E - E_l). \tag{3}$$

$\theta(E)$ represents the Heaviside step function and the $c_i$ $(i = 1, \dots, l)$ weight the contributions of the individual steps. The dimension of the square-root part has been reduced from 3D to 2D by introducing an effective length $L$ involved in the coefficient $c_l$ that describes the extension of occupied 3D states above the QW potential $E_l$ along the growth direction. In the case of parabolic energy bands with effective masses $m_i$ the coefficients $c_i$ are given by

$$c_i = \frac{m_i k_B}{\pi \hbar^2}, \quad i < l, \quad c_l = L \frac{(2 m_l k_B)^{3/2}}{2\pi^2 \hbar^3}, \tag{4}$$

where $k_B$ denotes the Boltzmann constant. It should be mentioned that $c_i$ $(i < l)$ and $c_l$ have different units $\mathrm{m^{-2}\,K^{-1}}$ and $\mathrm{m^{-2}\,K^{-3/2}}$, respectively. Inserting Eq. (3) into Eqs. (1) and (2) we obtain in Boltzmann approximation $(E - \mu \gg k_B T)$:

$$N_i = \left( \sum_{j=1}^{i} c_j \right) T \left( e^{-(E_i - \mu)/k_B T} - e^{-(E_{i+1} - \mu)/k_B T} \right), \quad i < l, \tag{5}$$

$$N_l = \left( \sum_{j=1}^{l-1} c_j + c_l T^{1/2} \right) T e^{-(E_l - \mu)/k_B T}. \tag{6}$$

The chemical potential $\mu$ can be eliminated dividing $N_i$ and $N_l$ by $N_1$:

$$\frac{N_i}{N_1} = \left( \sum_{j=1}^{i} C_j \right) \frac{e^{-\Delta E_i / k_B T} - e^{-\Delta E_{i+1}/k_B T}}{1 - e^{-\Delta E_2 / k_B T}} = \Phi_i(T), \quad i < l, \tag{7}$$

$$\frac{N_l}{N_1} = \left( \sum_{j=1}^{l-1} C_j + C_l T^{1/2} \right) \frac{e^{-\Delta E_l / k_B T}}{1 - e^{-\Delta E_2 / k_B T}} = \Phi_l(T), \tag{8}$$

with

$$C_j = \frac{c_j}{c_1} \ , \quad \Delta E_i = E_i - E_1 \ . \tag{9}$$

For parabolic bands we obtain

$$C_l = L \frac{(2k_B)^{1/2} m_l^{3/2}}{\pi \hbar m_1}, \quad C_j = \frac{m_j}{m_1}, \quad j < l. \tag{10}$$

This model for a 2D DOS may be compared with the simpler model for a $\delta$-shaped DOS frequently used in the literature to derive activation energies:

$$D^{\delta}(E) = \sum_{i=1}^{l} c_i \delta(E - E_i). \tag{11}$$

In this case the occupation ratios $\Phi_i$ from Eqs. (7) and (8) read

$$\Phi_i(T) = C_i e^{-\Delta E_i / k_B T} \ , \quad i = 1, ..., l \ . \tag{12}$$

So far our considerations are independent of the charge-carrier type, and the results from Eqs. (7), (8), and (12) are valid for both electron densities $n_i$ $(i =$

$1,\ldots,l$) in a conduction-band QW and hole densities $p_j$ ($j = 1,\ldots,m$) in a valence-band QW. The confinement energies of electrons and holes are denoted by $E_{ni}$ ($i = 1,\ldots,l$) and $E_{pj}$ ($j = 1,\ldots,m$), respectively, with QW potential depths $E_{nl}$ and $E_{pm}$. In PL experiments excess carrier densities $\delta n$ and $\delta p$ are optically generated in the semiconductor in addition to the equilibrium electron density $n_0$ and hole density $p_0$. Therefore, we have

$$n_i = n_{0i} + \delta n_i \ , \quad p_j = p_{0j} + \delta p_j . \tag{13}$$

The intensity $I_{\rm PL}$ of QW photoluminescence arising from the radiative transition between the lowest electron and hole subbands is given by

$$\begin{aligned} I_{\rm PL} &\sim r_{11}^R (n_1 p_1 - n_{01} p_{01}) \\ &= r_{11}^R (n_{01}\delta p_1 + \delta n_1 p_{01} + \delta n_1 \delta p_1), \end{aligned} \tag{14}$$

where $r_{11}^R$ denotes the radiative recombination coefficient. In general $r_{11}^R$ is temperature dependent. Calculations have shown that $r_{11}^R$ is proportional to $T^{-3/2}$ in bulk material[21,22] and proportional to $T^{-1}$ in 2D material.[23–28]

In the following we restrict our considerations to the case of $n$-type material, where $N_D \approx n_0$ denotes the equilibrium density of free electrons, which is valid in the temperature range of PL loss, $T > 100$ K. These carriers are produced by the ionization of shallow donors in the bulk or QW material and are trapped in the QW. Then Eq. (14) becomes

$$I_{\rm PL} \sim r_{11}^R (N_{D1} + \delta n_1)\delta p_1 , \tag{15}$$

with $N_{D1} \approx n_{01}$. The term $\delta n_1 p_{01}$ has been neglected since $p_0$ is very small compared to both $\delta p$ and $N_D$. Similar considerations are valid for $p$-type material.

The temperature and time dependence of $I_{\rm PL}$ can be derived from a simple rate equation describing the change of the total excess electron and hole densities $\delta n$ and $\delta p$, respectively, with time:

$$\frac{d}{dt}\delta n = \frac{d}{dt}\delta p = g - \sum_{i=1}^{l}\sum_{j=1}^{m} r_{ij}(N_{Di} + \delta n_i)\delta p_j , \tag{16}$$

where charge neutrality, $d\delta n/dt = d\delta p/dt$, applies for bimolecular recombination processes. The optical generation of electron-hole pairs is represented by the generation rate $g$ and the radiative ($R$) or nonradiative (NR) recombination between electron states $i = 1,\ldots,l$ and hole states $j = 1,\ldots,m$ is described by the recombination coefficients

$$r_{ij} = r_{ij}^R + r_{ij}^{\rm NR} . \tag{17}$$

Using Eq. (7) and (8) we have

$$N_{Di} = N_{D1}\Phi_{ni}, \quad \delta n_i = \delta n_1 \Phi_{ni}, \quad \delta p_j = \delta p_1 \Phi_{pj} . \tag{18}$$

Therefore, Eq. (16) can be rewritten in the form

$$\begin{aligned} \frac{d}{dt}\delta n &= \frac{d}{dt}\delta p \\ &= g - r_{11}^R (N_{D1} + \delta n_1)\delta p_1 \sum_{i=1}^{l}\sum_{j=1}^{m} R_{ij}\Phi_{ni}\Phi_{pj} , \end{aligned} \tag{19}$$

with $R_{ij} = r_{ij}/r_{11}^R = (r_{ij}^R + r_{ij}^{\rm NR})/r_{11}^R$.

### A. Continuous-wave excitation

Under steady-state conditions the generation of electron-hole pairs is balanced by their recombination:

$$\frac{d}{dt}\delta n = \frac{d}{dt}\delta p = 0 . \tag{20}$$

Inserting Eqs. (15) and (20) into Eq. (19) we obtain, for the PL intensity of $(e_1 - h_1)$ QW transitions,

$$I_{\rm PL} \sim g \left[ \sum_{i=1}^{l}\sum_{j=1}^{m} R_{ij}\Phi_{ni}\Phi_{pj} \right]^{-1} . \tag{21}$$

According to Eq. (21) we expect the same temperature dependence of $I_{\rm PL}$ for both low injection ($\delta n, \delta p \ll N_D$) and high injection ($\delta n, \delta p \gg N_D$). This result is a consequence of the model assumption that both the optically created carrier densities $\delta n$, $\delta p$ and the extrinsic carrier density $N_D$ are distributed in energy according to Eqs. (7) and (8) irrespective of their different origin. If, e.g., electrons from the background doping $N_D$ would not be taken into account in the thermal carrier distribution and a low optical excitation is assumed, then the dominant recombination term would be $N_D \delta p$ and holes alone would govern the decay kinetics with their associated hole binding energy.

In the model outlined the recombination term $r_{lm}(N_{Dl} + \delta n_l)\delta p_m$ in Eq. (16) describes recombination between continuous electron and hole states including nonradiative surface or interface recombination. According to the familiar selection rules optical transitions with $i \neq j$ ($i < l, j < m$) are forbidden in an ideal square-well potential QW and the corresponding recombination coefficients $r_{ij}$ should be zero. However, nonradiative recombination between electronic states at the interfaces[29–33,1,34,35] is allowed, and therefore the coefficients $r_{ij}$ may be nonzero.

### B. Pulsed excitation

In TR experiments the system is excited ideally by a $\delta$ pulse at $t$=0 and the excess electron and hole densities decay to their equilibrium values at a rate determined by the total recombination coefficients $r_{ij}$:

$$\frac{d}{dt}\delta n = \frac{d}{dt}\delta p = -r_{11}^R (N_{D1} + \delta n_1)\delta p_1 \sum_{i=1}^{l}\sum_{j=1}^{m} R_{ij}\Phi_{ni}\Phi_{pj} . \tag{22}$$

For high excitation ($\delta n \gg N_D$) the decay of $\delta n$ and $\delta p$ is nonexponential immediately after switching off the external light source. However, for long times $t \geq t_0$ the excess majority-carrier density becomes much smaller than its equilibrium value, i.e., $\delta n \ll N_D$, and Eq. (22) simplifies to a linear differential equation for the excess minority-carrier concentration $\delta p_1$:

$$\frac{d}{dt}\delta p_1 = -\delta p_1 r_{11}^R N_D \frac{\sum_{i=1}^{l}\sum_{j=1}^{m} R_{ij}\Phi_{ni}\Phi_{pj}}{\sum_{i=1}^{l}\sum_{j=1}^{m}\Phi_{ni}\Phi_{pj}}, \tag{23}$$

where the relations

$$\delta p = \delta p_1 \sum_{j=1}^{m}\Phi_{pj}, \qquad N_D = N_{D1}\sum_{i=1}^{l}\Phi_{ni} \tag{24}$$

have been used. Solving Eq. (23) we have

$$\delta p_1(t) = \delta p_1(t_0)e^{-t/\tau} \tag{25}$$

with

$$\tau = \frac{1}{r_{11}^R N_D}\frac{\sum_{i=1}^{l}\sum_{j=1}^{m}\Phi_{ni}\Phi_{pj}}{\sum_{i=1}^{l}\sum_{j=1}^{m} R_{ij}\Phi_{ni}\Phi_{pj}}. \tag{26}$$

Thus, for low excess carrier densities, the excess minority-carrier concentration decays exponentially with time constant $\tau$.

Using Eq. (15) with $\delta n \ll N_D$ we obtain, for the time-dependent PL intensity,

$$I_{\rm PL}(t) = I_{\rm PL}(t_0)e^{-t/\tau} \sim r_{11}^R N_{D1}\delta p_1(t). \tag{27}$$

### C. Discussion

Now let us focus on the temperature dependence of $I_{\rm PL}$ in Eq. (21) and $\tau$ in Eq. (26). Since in the measured PL spectra the intensities of $i \rightarrow j$ radiative transitions with $(i,j) \neq (1,1)$ are negligible in comparison to that of the fundamental transition $(i,j) = (1,1)$, we deduce $r_{ij} \approx r_{ij}^{\rm NR}$ for $(i,j) \neq (1,1)$, i.e., for all transitions except the fundamental one only nonradiative recombination processes are taken into account. This is surely valid for our samples with thin QW thicknesses and therefore large energy steps for confined QW states. All nonradiative recombination coefficients $r_{ij}^{\rm NR}$ are taken to be approximately temperature independent. For the radiative recombination coefficient $r_{11}^R$ a temperature dependence $r_{11}^R \sim T^{-1}$ is taken into account as cited above, yielding $R_{ij} \approx r_{ij}^{\rm NR}/r_{11}^R \sim T$ for $(i,j) \neq (1,1)$. The contribution of $r_{11}^{\rm NR}$ to the total recombination coefficient $r_{11}$ is not known. Therefore, the ratio $r_{11}^{\rm NR}/r_{11}^R$ in $R_{11} = 1+r_{11}^{\rm NR}/r_{11}^R$ is treated as a fit parameter. In Sec. III, Eqs. (21) and (26) will be used to model the experimental data.

In order to demonstrate the characteristic features of our theoretical model, Fig. 1 shows the intensity $I_{\rm PL}$ from Eq. (21) (dotted lines) and the lifetime $\tau$ from Eq. (26) (dashed lines) in an Arrhenius plot calculated for a fictitious QW. In Fig. 1(a) the 2D DOS from Eq. (3) and in Fig. 1(b) the $\delta$ DOS from Eq. (11) have been used. Only one confined state is taken for both electrons and holes (i.e., $l = m = 2$) with binding energies $\Delta E_{n2}$ = 120 meV and $\Delta E_{p2}$ = 80 meV, respectively. The following input parameters have been chosen for the graph: $R_{12} = R_{21} = 1T$ K$^{-1}$, $R_{22} = 100T$ K$^{-1}$, $C_{n2} = C_{p2}$ = 1 K$^{-1/2}$ (2D DOS), and $C_{n2} = C_{p2} = 10$ ($\delta$ DOS). Both $I_{\rm PL}$ and $\tau$ start to decrease with increasing temperature at around 100 K. Whereas the slope of $\ln(I_{\rm PL})$ vs $(1/T)$ steadily increases and does not reach any maximum, the slope of $\ln(\tau)$ vs $(1/T)$ reaches its maximum at $T \approx 300$ K and decreases again for higher temperatures. Fitting a simple exponential function $\exp(\Delta E/k_BT)$ to the high-temperature part of $I_{\rm PL}$ and $\tau$, as usually done for experimental temperature-dependent data, the total binding energy $\Delta E_{\rm tot}$ = 200 meV is not correctly delivered. The slope $\Delta E$ turns out to be larger than $\Delta E_{\rm tot}$ for $I_{\rm PL}$ (236 meV, 203 meV) and lower than $\Delta E_{\rm tot}$ for $\tau$ (165 meV, 149 meV) for both the 2D DOS and the $\delta$ DOS. The difference between the temperature dependences of $I_{\rm PL}$ and $\tau$ can be understood by analyzing the relation

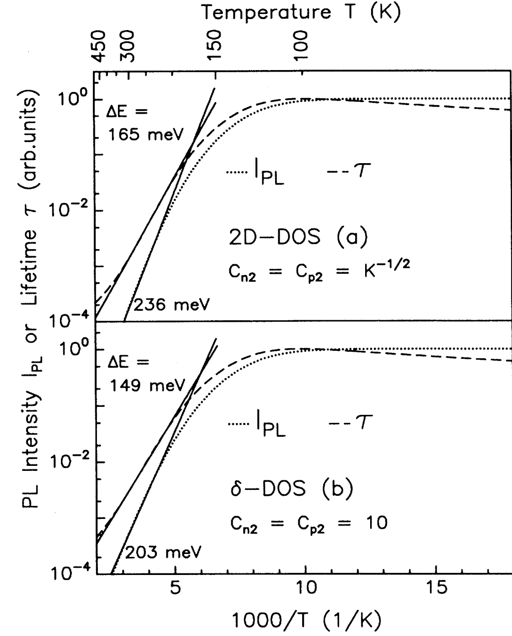


FIG. 1. Model calculations of $I_{\rm PL}$ (doted lines) and $\tau$ (dashed lines) using Eq. (21) and (26), respectively, with $l = m = 2$ for a 2D DOS (a) and a $\delta$ DOS (b). Slope values $\Delta E$ of the curves in the high-temperature limit were obtained from fitting simple exponentials $\sim \exp(\Delta E/k_BT)$ (solid lines) to the calculated curves.

$$\tau = \frac{\sum_{i=1}^{l}\sum_{j=1}^{m}\Phi_{ni}\Phi_{pj}}{g r_{11}^R N_D} I_{\rm PL}, \tag{28}$$

obtained from Eqs. (21) and (26). The exponential functions in the numerator and the radiative recombination coefficient $r_{11}^R \sim T^{-1}$ in the denominator lead to a weaker decrease of $\tau$ with increasing temperature compared to $I_{\rm PL}$. In order to extract the dominating term of $I_{\rm PL}$ in the high-temperature limit the inequality

$$R_{lm}C_{nl}C_{pm} \gg R_{ij}C_{ni}C_{pj}, \quad i < l, j < m \qquad (29)$$

is applied to Eq. (21). It holds for high temperatures whenever effective nonradiative recombination processes are present in the barrier material. In the simple case of a $\delta$-shaped DOS $I_{\rm PL}$ becomes

$$I^{\delta}_{\rm PL} \sim \frac{g}{R_{lm}C_{nl}C_{pm}} e^{\Delta E_{\rm tot}/k_BT}. \qquad (30)$$

Taking into account the temperature dependence of $R_{lm} \sim T$ an activation energy slightly larger than the total binding energy $\Delta E_{\rm tot} = \Delta E_{nl} + \Delta E_{pm}$ is obtained from the slope of $\ln(I_{\rm PL})$ vs $(1/T)$. Considering the more realistic 2D DOS Eq. (30) becomes

$$I^{\rm 2D}_{\rm PL} \sim \frac{g[1 - e^{-\Delta E_{n2}/k_BT}][1 - e^{-\Delta E_{p2}/k_BT}]}{R_{lm}\left[\sum_{i=1}^{l-1} C_{ni} + C_{nl}T^{1/2}\right]\left[\sum_{j=1}^{m-1} C_{pj} + C_{pm}T^{1/2}\right]} \times e^{\Delta E_{\rm tot}/k_BT}. \qquad (31)$$

Here the dominant temperature-dependent term of the PL intensity is again given by $\exp[\Delta E_{\rm tot}/k_BT]$. However, the quenching of $I_{\rm PL}$ with increasing temperature is strengthened by the two exponential functions in the numerator and by $T$-dependent terms in the denominator. Thus, for both types of DOS, assuming $R_{lm} \sim T$, the resulting slope in an Arrhenius plot $\ln(I_{\rm PL})$ vs $(1/T)$ is larger than the total binding energy at high temperatures. As a conclusion we note that the activation energy of nonradiative recombination processes cannot be determined by fitting a simple exponential function $\exp(\Delta E/k_BT)$ to the experimental data of $I_{\rm PL}$ or $\tau$. On the contrary, a careful comparison has to be performed between calculated curves and measured data within an extended temperature range where $I_{\rm PL}$ or $\tau$ decrease by at least three orders of magnitude.

## III. MEASUREMENTS

### A. Experimental details

The CW PL spectra were recorded with excitation at 488-nm or 514-nm wavelength of an $\mathrm{Ar^+}$-ion laser at sample temperatures varied from 1.7 K to 400 K. The PL signals were dispersed by a 1-m grating monochromator and detected by a germanium photodiode cooled to 77 K or a Peltier cooled GaAs photomultiplier. The signals were processed by conventional lock-in techniques.

For the TR PL measurements with picosecond excitation we used a CW mode locked $\mathrm{Ar^+}$-ion laser followed by a synchronously pumped dye laser (pulse width 10 ps, $\lambda$ = 800 nm) with a repetition rate of 75.3 MHz. The PL signal was detected by a fast $S1$ microchannel plate. The experimental setup had an overall time resolution of about 50 ps.

Most of the PL investigations were carried out for different high and low excitation densities. In contrast to the TR case CW investigations exhibit a larger dynamic range in the observation of PL signals. Hence for CW excitation the PL intensities could be observed over an intensity range of more than three decades, and lifetimes could only be recorded over less than two decades.

### B. Results and discussion

Continuous-wave and time-resolved PL measurements were performed on four different samples grown by molecular-beam epitaxy (MBE) or metalorganic vapor-phase epitaxy (MOVPE). Sample 1 contains a MBE-grown pseudomorphic $\mathrm{In_{0.15}Ga_{0.85}As/GaAs}$ MQW structure with three QW's of thicknesses $L_z$ = 15 nm that are separated by GaAs barriers of 60-nm width (inset of Fig. 2). Sample 2 has nearly the same structure as sample 1 with the exception of two additional $\mathrm{Al_{0.38}Ga_{0.62}As}$ cladding barriers on both sides of the MQW structure (in-

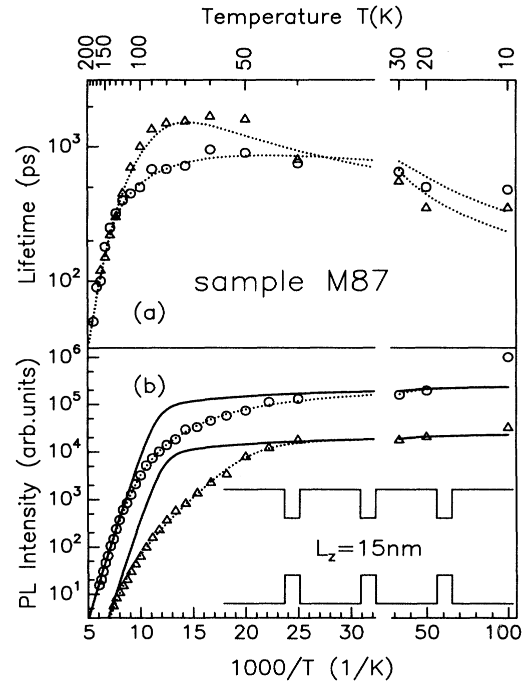


FIG. 2. Temperature dependence of PL lifetime (a) and intensity (b) for sample 1. The sample incorporates three QW's with $L_z$ = 15 nm separated by barriers of $L_B$ = 60 nm (inset). The measurements were performed at the two different excitation strengths of 0.3 $\mu$J/cm$^2$ (○) and 30 nJ/cm$^2$ (△) for TR, and 1 W/cm$^2$ (○) and 8 mW/cm$^2$ (△) for CW PL. The solid and dotted lines represent fits to the experimental data using (a) Eq. (26) and (b) Eq. (21). In order to achieve good agreement between experiment and theory very large recombination parameters $R_{ij}$ for the higher-lying confined QW states have to be assumed. In the case of the PL lifetime (a) we obtain $R_{22} = 1T$ K$^{-1}$ for low excitation and $R_{21} = 1T$ K$^{-1}$ for high excitation. The PL intensities shown in (b) were shifted vertically for comparison. Both curves are described by our theoretical model (dotted lines) with $R_{21} = 50T$ K$^{-1}$ and $R_{22} = 30T$ K$^{-1}$ for low excitation and $R_{21} = 20T$ K$^{-1}$ for high excitation. The curves drawn by solid lines are calculated with $R_{12} = R_{22} = 0.01T$ K$^{-1}$.

set of Fig. 3). These barriers prevent charge carriers from leaving the QW region. The three wells have identical thicknesses of $L_z = 10$ nm and are separated by barriers of 10-nm width. Sample 3 was grown by MBE and incorporates two coupled $GaAs/Al_{0.33}Ga_{0.67}As$ QW's of width 4 nm (QW1) and 7 nm (QW2) (inset of Fig. 4). The barrier between the wells has a thickness of 10 nm. Measurements were also performed on the MOVPE-grown MQW structure 4 containing six QW's of lattice matched $In_{0.53}Ga_{0.47}As/InP$. The QW's have widths of 0.3 nm, 0.6 nm, 1.1 nm, 2.5 nm, 4.8 nm, and 8.7 nm and barriers in between of 20 nm. In addition, the sample contains an $In_{0.53}Ga_{0.47}As$ control layer that is 110 nm wide.

For all samples under investigation the discrete QW energy levels $E_{ni}$ $(i < l)$, $E_{pj}$ $(j < m)$ and the associated activation energies $\Delta E_{ni} = E_{ni} - E_{n1}$ $(i = 1, \ldots, l)$, $\Delta E_{pj} = E_{pj} - E_{p1}$ $(j = 1, \ldots, m)$ were calculated from the known well potentials $E_{nl}$, $E_{pm}$ and the well widths $L_z$ using a transfer matrix method and taking into account 2D exciton binding energies.[36,37] The calculated values given in Table I match the experimental values from photoluminescence excitation (PLE) measurements at $T = 4.2$ K within a few meV.

The measured temperature dependence of the PL intensities $I_{\rm PL}$ and lifetimes $\tau$ were modeled using Eqs. (21) and (26), respectively. The occupation ratios $\Phi_{ni}$ and $\Phi_{pj}$ were taken from Eqs. (7) and (8) considering the DOS described by Eq. (3). Before presenting experimental data the values of the parameters used in the comparative calculations will briefly be summarized. The

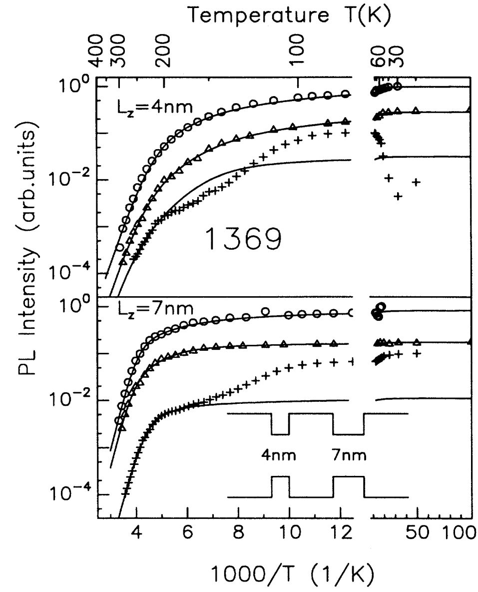


FIG. 4. Temperature dependence of PL intensities from QW1 (4 nm) and QW2 (7 nm) of sample 3. Shown are measurements for excitation densities of 2 mW/cm$^2$ (+), 320 mW/cm$^2$ (△), and 3 kW/cm$^2$ (○). The solid lines represent fits to the experimental data. For medium and high excitation densities $R_{13} \approx 10T$ K$^{-1}$ is used to fit the PL intensities of QW1.

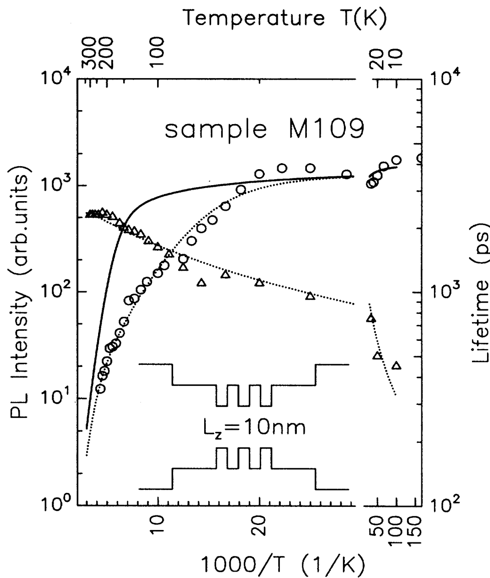


FIG. 3. Temperature dependence of PL intensity (○) and lifetime (△) for sample 2. The sample incorporates additional barriers to keep the carriers within the QW region. The excitation densities are 50 mW/cm$^2$ (CW) and 30 nJ/cm$^2$ (TR). The dotted lines represent fits to the experimental data. Used for the TR measurements were $R_{23} = R_{lm} = 10^{-3}T$ K$^{-1}$ and for the CW measurements $R_{23} = R_{lm} = 10^{-2}T$ K$^{-1}$ and $R_{12} = 0.5T$ K$^{-1}$. The solid curve is calculated for comparison with $R_{12} = 10^{-2}T$ K$^{-1}$.

steps $c_{ni}$ $(i < l)$ and $c_{pj}$ $(j < m)$ in the 2D DOS were assumed to be of equal height, respectively, resulting in $C_{ni} \approx C_{pj} \approx 1$ for $i < l, j < m$. A rough estimate of $C_{nl}$ and $C_{pm}$ using Eq. (10) yields $C_{nl} \approx C_{pm} \approx 1$ K$^{-1/2}$. Since it is essentially the product between $C_{ij}$ and $R_{ij}$ that appears in the formula of $I_{\rm PL}$ and $\tau$ the values of the $C_{ij}$ were held constant and the ratios $R_{ij} = r_{ij}/r_{11}^R$ were treated as fit parameters. If not stated otherwise we have obtained values in the range $r_{11}^{\rm NR}/r_{11}^R \leq 10^{-2}T$ K$^{-1}$, $1T$ K$^{-1} \leq R_{lm} \leq 10^5T$ K$^{-1}$, and $R_{ij} \leq 0.1T$ K$^{-1}$ for all other $R_{ij}$. The high values of $R_{lm}$ indicate that very effective nonradiative recombination channels are present in the barrier material, leading to a strong decrease of the PL intensity at high temperatures. Nonradiative transitions from spatially extended states above the QW potential to confined 2D states within the QW are assumed to be negligible and therefore the corresponding $R_{ij}$ are set to zero. However, this restriction has turned out to have no significant influence on the theoretical results. It should be emphasized that it is not the aim of this paper to deduce exact values for the parameters $C_{ni}$, $C_{pj}$, and $R_{ij}$. Therefore, only the orders of magnitude are given. These are sufficient for the discussion of our primary problem of carrier activation energies out of the QW's. The activation energies $\Delta E_{ni}$ $(i = 1, \ldots, l)$ and $\Delta E_{pj}$ $(j = 1, \ldots, m)$ of Table I were used as discussed above.

In Fig. 2 the temperature dependence of the PL lifetime $\tau$ and the PL intensity $I_{\rm PL}$ for the $In_{0.15}Ga_{0.85}As/GaAs$ MQW sample 1 is shown in an

TABLE I. Activation energies $\Delta E_{ni}$ and $\Delta E_{pj}$ of electrons and holes, respectively, used in our model to describe the temperature dependence of the PL intensity $I_{PL}$ and the lifetime $\tau$. The QW confinement energies $E_{ni}$ and $E_{pj}$ are calculated using the transfer-matrix method and are in good agreement with our data from PLE measurements at $T = 4.2$ K. $\Delta E_{nl}$ and $\Delta E_{pm}$ indicate the binding energies given by the difference between the QW potential and the lowest confinement energy, i.e., the QW ground state.

| Sample | Material system | $\Delta E_{ni} = E_{ni} - E_{n1}$ (meV) $(1 < i < l)$ | $\Delta E_{nl} = E_{nl} - E_{n1}$ (meV) |
|---|---|---|---|
| 1 | $In_{0.15}Ga_{0.85}As/GaAs$ | 37 | 61 |
| 2 | $In_{0.15}Ga_{0.85}As/GaAs$ | | 50 |
| 3 (QW1) | $GaAs/Al_{0.33}Ga_{0.67}As$ | | 142 |
| 3 (QW2) | $GaAs/Al_{0.33}Ga_{0.67}As$ | 139 | 196 |
| 4 | $In_{0.53}Ga_{0.47}As/InP$ | | 8 |

| Sample | $\Delta E_{pj} = E_{pj} - E_{p1}$ (meV) $(1 < j < m)$ | | | | $\Delta E_{pm} = E_{pm} - E_{p1}$ (meV) |
|---|---|---|---|---|---|
| 1 | 7 | 20 | 36 | | 45 |
| 2 | 20 | | | | 45 |
| 3 (QW1) | 37 | 97 | | | 125 |
| 3 (QW2) | 22 | 43 | 109 | 117 | 144 |
| 4 | 75 | | | | 92 |

Arrhenius-type plot. For the CW measurements [Fig. 2(b)] two different excitation densities of $8 \mathrm{mW/cm}^2$ (triangles) and $1 \mathrm{W/cm}^2$ (circles) were used. The measured PL intensities in Fig. 2(b) differ by a factor of 100 at low temperatures but have relatively been shifted vertically for a better comparison. For $T \leq 50$ K the PL intensities remain nearly constant until they drop at higher temperatures. The PL intensities could be measured over a range of four orders of magnitude for high excitation and over a range of three and a half orders for low excitation. It should be emphasized that the slopes of the experimental curves increase over the whole detectable intensity range of at least three orders of magnitude. The temperature-dependent behavior of the two curves is significantly different. In the case of high excitation the slope of the curve continuously increases with increasing temperature for 50 K $\leq T \leq$ 150 K and becomes nearly constant for $T \geq 150$ K. For low excitation the slope strongly increases at $T \approx 50$ K and is nearly constant between 50 K and 80 K. For higher temperatures the slope increases again, but it does not match the maximum value of the high excitation curve within the temperature range accessible to observation. Using values for the recombination coefficients $R_{ij}$ as given above the experimental curves can be well described by our theoretical model only in the limit of low and high temperatures (solid lines). In the temperature range 50 K $\leq T \leq$ 150 K a satisfying fit to the experimental data can only be obtained if unreasonably large recombination coefficients are chosen for some of the higher-lying confined QW states (dotted lines). Therefore, we are led to the assumption that there may exist further nonradiative recombination channels with an activation energy lower than the total binding energy $\Delta E_{\mathrm{tot}}$ and independent of the QW energy levels. Similar observations have already been made by other groups.[13,16,20] Since the feature of weak PL decrease is less pronounced for high than for low excitation density these recombination channels seemingly saturate with increasing excitation density. The origin of these competing recombination processes is not yet known. However, nonradiative recombination at interface states between QW and barrier has widely been suggested to be responsible for the observed behavior of $I_{PL}$ at medium temperatures.[4,5,15,29,30,32,33]

In Fig. 2(a) the temperature dependence of PL lifetime $\tau$ is depicted for excitation pulses with low energies of 30 $\mathrm{nJ/cm}^2$ (triangles) and high energies of 0.3 $\mu\mathrm{J/cm}^2$ (circles). In the case of low excitation (triangles) the lifetime increases with increasing temperature for $T \leq 50$ K and drops exponentially for $T \geq 100$ K. At low temperatures charge carriers are trapped within the QW and the increase of lifetime $\tau$ mainly reflects the $T^{-1}$ temperature dependence of the recombination coefficient $r_{11}^R$. At increasing temperature states with energies above the QW potentials $E_{nl}$ and $E_{pm}$ are occupied and nonradiative transitions from these states lead to a strong decrease of the PL lifetime $\tau$. For high excitation (circles) the increase of $\tau$ between 4.2 K and 50 K is less pronounced than for low excitation. This may be due to a saturation of the radiative recombination channel. For both excitation densities the temperature dependence of $\tau$ can be well described within our model (dotted lines) using Eq. (26) with the same parameters $C_{ni}$ and $C_{pj}$ as for the CW investigations. However, the recombination coefficients $R_{ij}$ have to be modified, which may be due to different recombination kinetics for CW and pulsed excitation.

The temperature dependence of the PL lifetime $\tau$ (triangles) and the intensity $I_{PL}$ (circles) of sample 2 are depicted in Fig. 3. The inset of Fig. 3 schematically shows the conduction-band and valence-band potentials along the growth direction. The temperature dependence of both PL lifetime and PL intensity is significantly different from those of sample 1 within the temperature range 4.2 K $\leq T \leq$ 300 K. The PL intensity decreases only by two orders of magnitude and the PL lifetime monotonuously increases over the whole temperature range. In compar-

ison to sample 1 the QW's of sample 2 are thinner and hence the binding energies are smaller. Therefore, without any cladding barriers the drop of PL intensity and lifetime would be expected to occur at even lower temperatures than in sample 1. However, the $Al_xGa_{1-x}As$ cladding barriers on both sides of the MQW structure play an important role for the reduction of carrier loss channels. Carriers thermally activated into continuous QW or barrier states are reflected at the cladding barriers and are therefore hindered from leaving the QW region. Thus, nonradiative recombination processes in the barrier material such as surface recombination are suppressed to a large extent and the decrease of $I_{\rm PL}$ and $\tau$ with increasing temperature is weakened. This behavior is reflected in the very low values of the recombination coefficients $R_{lm}$ for transitions between unbound electron and hole QW states above the well potential necessary for good fits to the experimental data (dotted lines). These values are smaller by a factor of $10^4$ to $10^6$ compared to those of sample 1. Analogously to Fig. 2(b), the solid curve in Fig. 3 is calculated for comparison with very small coefficients $R_{ij} = 10^{-2}T$ K$^{-1}$ representing recombinations between higher-lying bound states. Values larger by several orders of magnitude have to be used to obtain the dotted curve. This demonstrates that the weak decrease of the PL intensity in the temperature range 80 K $\leq T \leq$ 200 K cannot be explained by nonradiative recombination between electron and hole barrier states.

In Fig. 4 the temperature dependent PL intensities from QW1 and QW2 of sample 3 are shown for the three different excitation densities 3 kW/cm$^2$ (circles), 320 mW/cm$^2$ (triangles), and 2 mW/cm$^2$ (crosses). For high and medium excitation the results are similar to those of sample 1 and can be modeled satisfactorily. However, for the extremely low excitation density of 2 mW/cm$^2$ a qualitatively different behavior is found. There is an additional step between 150 K and 200 K for both QW's. With increasing excitation density this step is smeared out. Furthermore, there is a second unusual feature at 2 mW/cm$^2$ excitation density around 80 K where QW1 exhibits an abrupt jump of a factor 10 in the PL intensity. Such temperature behavior has not been found in any other QW PL. Obviously, there are processes which are not contained in our model. Therefore, in this case the model cannot describe correctly the observed temperature dependence of the intensities. The final, strong intensity decrease at high temperatures is common to all excitation densities. Again, the curves can be well fitted using as thermal activation energies the total binding energy $\Delta E_{\rm tot}$ of electrons and holes in the QW.

Next, we have studied the thinnest QW ($L_z = 0.3$ nm) of sample 4 which incorporates six QW's in total and was grown by MOVPE. The temperature dependence of the PL intensity and the PL lifetime of that QW are shown in Fig. 5. The corresponding data of the other five QW's are dominated by vertical carrier transport across the InP barriers from thinner into broader QW's and will be reported elsewhere. In this paper we focus on the QW with $L_z = 0.3$ nm. The PL intensity has been studied for excitation densities of 240 $\mu$W/cm$^2$, 210 mW/cm$^2$, 1.2 W/cm$^2$, and 30 W/cm$^2$. The PL signal could be detected over an intensity range of two decades. Independent of the excitation level, all decay curves have identical high-temperature slopes that are associated with the total binding energy $\Delta E_{\rm tot}$. In contrast to the MBE-grown samples 1, 2, and 3, no weak initial decrease of $I_{\rm PL}$ is observed in this MOVPE-grown sample. With our assumption that recombination centers at the QW interface are responsible for the PL decrease at medium temperatures, the lack of this decrease may be the consequence of an excellent crystal quality reducing the strength of nonradiative recombination at the interfaces between $In_{0.53}Ga_{0.47}As$ and InP. The only difference between the intensity curves is a steady shift of the threshold temperature where the intensity begins to drop. Within our model this shift can be well reproduced by reducing the value of $R_{lm}$. This indicates that the dominating nonradiative recombination processes in the barrier material described by $R_{lm}$ are saturable. The drop of the PL lifetime $\tau$ (excitation energy 30 nJ/cm$^2$) versus temperature is almost identical to that of $I_{\rm PL}$. Good agreement between experiment and theory (solid line) is achieved if nonradiative transitions between bound QW states are neglected.

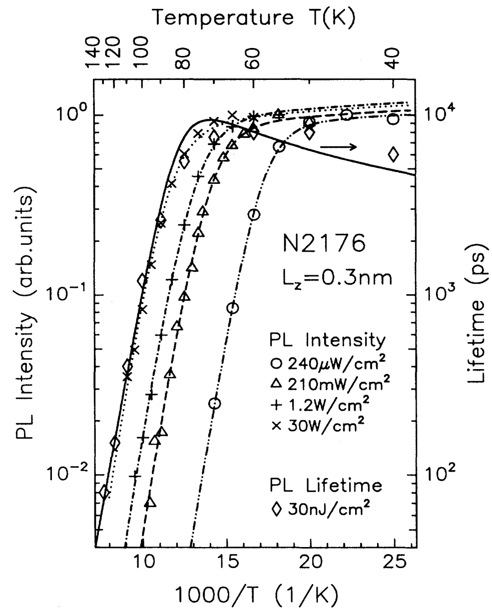


FIG. 5. Temperature dependence of PL intensities and lifetimes from the thinnest QW ($L_z$ = 0.3 nm) of sample 4. The PL intensities were recorded with four different excitation densities. The lines represent fits to the experimental data.

## IV. CONCLUSION

Temperature-dependent CW and time-resolved PL measurements were performed on QW's in different material systems for both high and low excitation den-

sities. For all samples with the exception of the $In_{0.53}Ga_{0.47}As/InP$ sample it was shown that the decrease of the PL intensities with increasing temperature can be separated into two ranges. In the first range, at medium temperatures, the PL intensity decreases by about two orders of magnitude. Here, an Arrhenius-type plot yields an activation energy smaller than the total binding energy of electrons and holes. This range is most pronounced for low excitation densities. In the second range, at high temperatures, the drop of PL intensity is strong and the corresponding activation energy is associated with the total binding energy of electrons and holes. The experimental data for both CW and time-resolved measurements can be well fitted within a theoretical model where electrons and holes are distributed in energy according to Fermi-Dirac statistics assuming a steplike two-dimensional density of states and radiative or nonradiative recombination between QW or barrier states, respectively. However, unreasonably large recombination coefficients have to be used for the nonradiative transition between some of the higher-lying QW states in order to model the PL intensity in the first temperature range. This leads to the conclusion that further recombination channels exist, presumably located at the interface between QW and barrier, with an activation energy lower than the total binding energy $\Delta E_{tot}$ and independent of QW energy levels. In the $In_{0.53}Ga_{0.47}As/InP$ sample the first range of weak PL decrease does not appear and both PL intensity and lifetime decrease only with the total binding energy. This is attributed to the high crystal quality of this sample. Theoretical considerations and experimental data have been used to conclude that in the high-temperature limit the final drop of PL intensities and lifetimes is associated with the total binding energy of electrons and holes independent of the material system and the excitation density.

---

* Present address: ANT Nadwichtentechnik GmbH Bosch Telekom AN/EVO/51, Gerberstraße 33, 71520 Backnang, Germany.


[1] Y. J. Ding, C. L. Guo, S. Li, J. B. Khurgin, K.-K. Law, and J. L. Merz, Appl. Phys. Lett. **60**, 154 (1992).

[2] J. V. D. Veliadis, Y. J. Ding, J. B. Khurgin, and D. K. Wickenden, J. Lumin. **63**, 55 (1995).

[3] V. Srinivas, J. Hryniewicz, Y. J. Chen, and C. E. C. Wood, Phys. Rev. B **46**, 10 193 (1992).

[4] M. Krahl, D. Bimberg, and R. K. Bauer, J. Appl. Phys. **67**, 434 (1990).

[5] H. Hillmer, A. Forchel, R. Sauer, and C. W. Tu, Phys. Rev. B **42**, 3220 (1990).

[6] F. Martelli, M. G. Proietti, M. G. Simeone, M. R. Bruni, and M. Zugarini, J. Appl. Phys. **71**, 539 (1992).

[7] M. Gurioli, A. Vinattieri, M. Colocci, J. Massies, G. Neu, A. Bosacchi, and S. Franchi, Phys. Rev. B **44**, 3115 (1991).

[8] M. Gurioli, J. Martinez-Pastor, M. Colocci, C. Deparis, B. Chastaingt, and J. Massies, Phys. Rev. B **46**, 6922 (1992).

[9] P. Michler, A. Hangleiter, M. Moser, M. Geiger, and F. Scholz, Phys. Rev. B **46**, 7280 (1992).

[10] J. P. Bergman, P. O. Holtz, B. Monemar, M. Sundaram, J. L. Merz, and A. C. Gossard, Mater. Sci. Forum **143-147**, 117 (1994).

[11] G. Bacher, H. Schweitzer, J. Kovaç, A. Forchel, H. Nickel, W. Schlapp, and R. Lösch, Phys. Rev. B **43**, 9312 (1992).

[12] G. Bacher, C. Hartmann, H. Schweizer, T. Held, G. Mahler, and H. Nickel, Phys. Rev. B **47**, 9545 (1993).

[13] J. D. Lambkin, D. J. Dunstan, K. P. Homewood, L. K. Howard, and M. T. Emeny, Appl. Phys. Lett. **57**, 1986 (1990).

[14] S. Marcinkevičius, U. Olin, and G. Treideris, J. Appl. Phys. **74**, 3587 (1993).

[15] M. Vening, D. J. Dunstan, and K. P. Homewood, Phys. Rev. B **48**, 2412 (1993).

[16] J. R. Botha and A. W. R. Leitch, Phys. Rev. B **50**, 18 147 (1994).

[17] S. Weber, W. Limmer, K. Thonke, R. Sauer, T. Baier, D. Geiger, H. P. Meier, and K. Panzlaff, in *Growth, Processing, and Characterization of Semiconductor Heterostructures*, edited by G. Gumbs, S. Luryi, B. Weiss, and G. W. Wicks, MRS Symposia Proceedings No. 326 (Materials Research Society, Pittsburgh, 1994), p. 487.

[18] K. Fujiwara, N. Tsukada, T. Nakayama, and N. Nakamura, Phys. Rev. B **40**, 1096 (1989).

[19] J. A. Cavailles, D. A. B. Miller, J. E. Cunningham, P. L. K. Wa, and A. Miller, Appl. Phys. Lett. **61**, 426 (1992).

[20] H. Schneider and K. v. Klitzing, Phys. Rev. B **38**, 6160 (1988).

[21] R. N. Hall, Proc. Inst. Elect. Eng. **106B** Suppl. 17, 983 (1960).

[22] D. Z. Garbuzov, J. Lumin. **27**, 109 (1982).

[23] Y. Arakawa, H. Sakaki, M. Nishioka, J. Yoshino, and T. Kamiya, Appl. Phys. Lett. **46**, 519 (1985).

[24] J. Martinez-Pastor, A. Vinattieri, L. Carraresi, M. Colocci, Ph. Roussignol, and G. Weimann, Phys. Rev. B **47**, 10 456 (1993).

[25] P. J. Bishop, M. E. Daniels, B. K. Ridley, and K. Woodbridge, Phys. Rev. B **45**, 6686 (1992).

[26] A. Haug, Appl. Phys. B **44**, 151 (1987).

[27] J. Feldmann, G. Peter, E. O. Göbel, P. Dawson, K. Moore, C. Foxon, and R. J. Elliott, Phys. Rev. Lett. **59**, 2337 (1987).

[28] T. Matsusue and H. Sakaki, Appl. Phys. Lett. **50**, 1429 (1987).

[29] P. Dawson and K. Woodbridge, Appl. Phys. Lett. **45**, 1227 (1984).

[30] G. Duggan, H. I. Ralph, and R. J. Elliott, Solid State Commun. **56**, 17 (1985).

[31] G. Bastard, C. Delalande, M. H. Meynadier, P. M. Frijlink, and M. Voos, Phys. Rev. B **29**, 7042 (1984).

[32] W. Pickin and J. P. R. David, Appl. Phys. Lett. **56** 268 (1990).

[33] J. E. Fouquet and A. E. Siegman, Appl. Phys. Lett. **46**, 280 (1985).

[34] P. O. Holtz, Q. X. Zhao, B. Monemar, M. Sundaram, J. L. Merz, and A. C. Gossard, Phys. Rev. B **50**, 4139 (1994).

[35] J. P. Bergman, P. O. Holtz, B. Monemar, M. Sundaram, J. L. Merz, and A. C. Gossard, Phys. Rev. B **43**, 4765 (1991).

[36] M. Grundmann and D. Bimberg, Phys. Rev. B **38**, 13 486 (1988).

[37] J. A. Brum and G. Bastard, J. Phys. C **18**, L789 (1985).